IET Optoelectronics

Research Article

IET Journals
The Institution of Engineering and Technology

Parametric study of 1310 nm ridge waveguide AlGaInAs-InP semi-conductor laser dynamics

ISSN 1751-8768
Received on 2nd February 2015
Revised on 10th April 2015
Accepted on 17th May 2015
doi: 10.1049/iet-opt.2015.0011
www.ietdl.org

Horacio I. Cantú[1] ✉, *Andrew McKee*[1], *Iain Eddie*[1], *Anthony E. Kelly*[2]

[1]*CST-Global Ltd., 4 Stanley Boulevard, Hamilton International Tech Park, High Blantyre, Hamilton, G72 0BN, UK*
[2]*School of Engineering, University of Glasgow, Rankine Building, G12 8LT, UK*
✉ *E-mail: hcantu@compoundsemi.co.uk*

Abstract: Dynamic performance of directly modulated Fabry–Pérot lasers is presented in this work subject to variation of parameters such as cavity length and facet reflectivity. This study is focused on the effect that physical parameters have on the slope of the laser resonance frequency against the square root of the injection current. Temperature variation is also studied to determine modulation bandwidth available for high speed device operation at 10 Gbps. The effect of facet reflectivity and temperature over the laser spectrum and wavelength is also discussed.

1 Introduction

Communications via optical fibres in short-range schemes such as fibre to the home require low complexity components that are capable to transmit information at multi-gigabit per second data-rates. Deployment of gigabit capable passive optical networks (GPON) is dependent on the use of a reliable light source that can be adapted to the wavelength, power and dynamics required for efficient uncooled operation. Fabry–Pérot (FP) lasers are relatively simple to fabricate, and can be directly modulated at high speed rates with a tolerable chromatic dispersion at short ranges [1]. In this study, the experimental dynamic characteristics of FP lasers based on the strained AlGaInAs-InP system are described for a number of parameter changes in the laser cavity design and operation conditions. The studied parameters are mainly: cavity length, facet coatings and temperature.

FP lasers are less expensive to fabricate than other existing solutions such as the distributed feedback (DFB) laser and the laser integrated electro-absorption modulator. AlGaInAs lasers have been shown to be reliable at high temperatures [2] and capable to operate within the wavelength specification (1310 nm) required for GPON upstream transmission.

Design of a directly modulated high-speed laser is not only a task that involves careful consideration of radio frequency (RF) effects and parasitics, but has also become a challenge in fulfilling the demands of uncooled communication applications. It is expected that specifications of the dynamic performance will be met in a broad range of temperatures, which makes reliability assurance under these conditions obligatory.

A number of scientific works have been previously conducted to understand semi-conductor laser dynamics for uncooled telecommunication applications. Many of the works have been concentrated on the operation of DFBs, which, as mentioned earlier, are more expensive to fabricate than FP lasers. Nakahara *et al*. [3] for example, demonstrated operation of a ridge waveguide DFB laser based on the AlGaInAs system, capable of data transmission at a rate of 12 Gbps. Other authors have concentrated their efforts on integrated epitaxial structures that are more complex and perform functions such as spot size conversion [4]. The work in [5] presented a summary of publications describing laser designs for 10 Gbps communication applications. Most of the designs summarised in [5] are based in the InGaAsP system with DFB laser structures. In this work, for the first time, a more intensive experimental characterisation of AlGaInAs-based FP laser dynamics is presented, which describes the effect of physical device parameters in their modulation efficiency.

The devices used in this work are production FP lasers fabricated at compound semi-conductor technologies (CST Global), which is a leading provider of laser sources for telecommunication applications. The characterisation of the designs used in this study has been organised in the following way: In Section 2, the general aspects and static performance of the lasers is described. Section 3 includes the lasers spectral output and the effect of facet coatings and temperature on the centre wavelengths. Section 4 describes the laser dynamics subjected to changes in cavity lengths, facet coatings and temperature. In the same section, eye diagrams resulting from data transmission are presented. A brief discussion on reliability and life test performance is included at the end of Section 4. Conclusions of this study are presented in Section 5.

2 Characteristics of ridge waveguide FP laser

The comprehensive design of AlGaInAs-InP strained multi-quantum well (MQW) epitaxial structures has been previously demonstrated to facilitate uncooled operation of lasers that operate at the wavelength required for optical communication systems. This epitaxial structure is successful because of a reduced carrier leakage from the quantum-well regions, a reduction of the transparency current and also of the carrier density dependence loss [6]. In this study, the active layers of the FP lasers are formed by a stack of quantum wells using the AlGaInAs-InP strained system. For high speed operation, it is important to increase the optical confinement factor provided by the active layers [7], and for that reason a high number of quantum wells are used in the FP lasers epitaxial structure design.

The laser hetero-structure in this work is grown using the metalorganic vapour phase epitaxy technique and is formed by several controlled growth sections: a highly p-doped (Zn) GaInAs electrode; an InP p-doped cladding structure; an AlGaInAs p-doped (Zn) transition layer; an active region consisting of tensely strained AlGaInAs quantum barriers and compressively strained AlGaInAs quantum wells; AlGaInAs n-doped (Si) transition layers; and the semi-conductor n-doped (Si) InP substrate. The total thickness of the p-electrode and cladding layer is approximately 1.8 μm. The total thickness of the un-doped active region is 145 nm. The number and thickness of quantum wells and barriers has been optimised to increase the differential gain of the laser [7], while taking account carrier transport across the separate confinement heterostructures [8], which effectively reduce the differential gain and effectively increase the differential carrier lifetime [8]. Development of a formal epitaxial structure

© The Institution of Engineering and Technology 2015

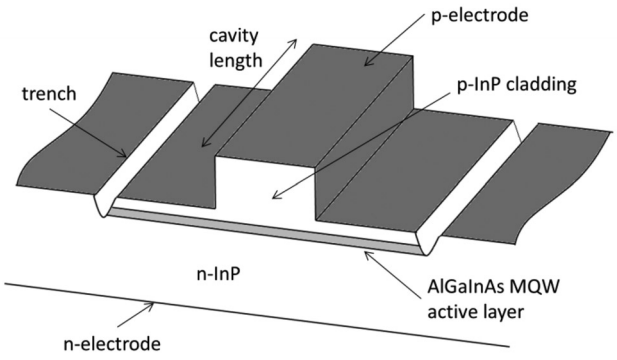

Fig. 1 *Schematic illustration of the ridge waveguide FP lasers used in this work*

optimisation procedure is still on-going, with the current design based primarily on evaluation and selection of the best high speed experimental performance obtained after the growth of several variants of high speed heterostructures.

The FP laser cavities used in this work consist of ridge waveguide structures such as the one illustrated in Fig. 1. The ridge is fabricated on a semi-conductor InP substrate that is processed to produce single dice that are 200 μm wide and 100 μm thick. The ridge forms a waveguide that confines the laser generated light between the cladding and the strained MQW AlGaInAs active layer. The nominal ridge width used in this study was 2 μm.

A gold metallisation pattern covers the ridge and forms the p-electrode that allows pumping and laser action using an electrical injection current. The n-electrode is formed with a back side metallisation, which forms an electrical contact with the n-doped InP substrate, as shown in Fig. 1. An etched trench on each side of the ridge allows electrical isolation of the p-electrode contact from the rest of the die surface.

Each facet of the ridge is coated with either anti-reflective or highly reflective (HR) layers that allow control of lasing action parameters such as the current threshold, the wavelength and power output of the device. For most of the measurements performed in this study, the light output of the lasers is coupled into a lensed fibre aligned to one of the ridge waveguide coated facets. The facet coating is described here in terms of the product of the percentages of reflectivity from each facet (R_1R_2).

A typical performance of the FP laser device intensity against current (LI), and bias voltage against current (VI) is shown in Fig. 2. The measurement corresponds to a device that has a cavity length of 200 μm and a product of facet coat reflectivity $R_1R_2 = 0.14$. The measurements were taken at a temperature of 25°C and 85°C using a pulsed DC bias supply. Current threshold at room temperature is typically 10 mA, and will change with temperature depending on the reflectivity value of the facet coating implemented. Slope efficiency for these FP devices is 0.45 W/A at 25°C, and decreases to 0.35 W/A at 85°C. This decrease of efficiency is related to the role played by temperature in the distribution of electrons and holes in the conduction and valence bands [9] of the laser. Agrawal and Dutta [9] explain, at higher temperatures the carriers are distributed over a wider energy range, hence the maximum optical gain from the laser is reduced.

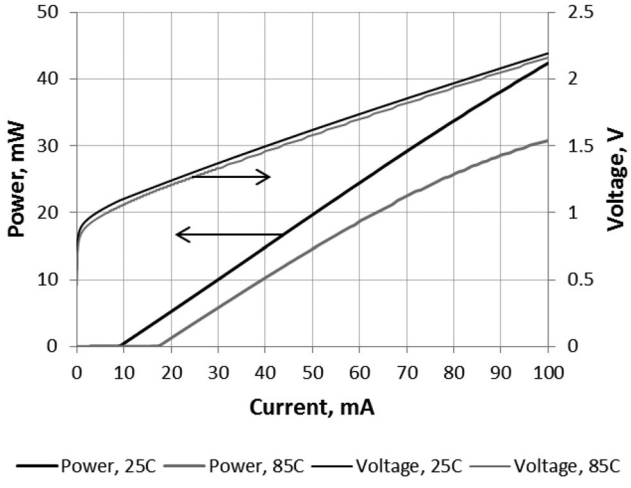

Fig. 2 *Measurements of LI and VI at two different temperature values for an FP laser with a 200 μm cavity length*

To perform the measurements shown in Fig. 2, a number of single FP laser dice were attached to AlN sub-mounts using eutectic bonding, and then wire bonded to the metallisation of the p-electrode of the devices. The output light was coupled to a broad area photo-detector using a tile test setup.

Laser series resistance is a relevant parameter for high speed applications because it has a significant role in determining the modulation bandwidth of directly modulated laser devices [10]. The FP lasers used in this work have typical resistances of 10, 11 and 13 Ω for the cases of 250, 200 and 150 μm laser cavity lengths, respectively.

3 Spectral characteristics in temperature

One of the requirements for uncooled communication applications of lasers is wavelength compliance under high temperature operation. A device that can achieve the dynamics required for transmission at multi giga-bit data rates will also require simultaneous compliance with wavelength under extreme temperature conditions. Fig. 3 shows the measured spectral output of a 200 μm cavity long ($R_1R_2 = 0.14$) FP laser at a temperature of 25°C and 85°C using 30 mA of injection current. The ratio of wavelength change and temperature change ($d\lambda/dT$) has been measured to be 0.5 nm/°C. This ratio implies a centre wavelength of 1340 nm at 85°C when a device active layer has been tuned for 1310 nm operation at room temperature.

The measured typical spectral widths for the FP devices ($R_1R_2 = 0.14$) were 1.5 nm at 25°C and 1.8 nm at 85°C.

Several experiments were performed to understand the relation between facet coatings, temperature and wavelength. Leaving the cavity length of the device constant at 200 μm, measurements of the centre wavelength were obtained using an optical spectrum analyser. A number of FP lasers were coated with R_1R_2 values of 0.14, 0.36 and 0.85, and the devices were tested at temperatures of 25°C, 50°C and 80°C. The R_1R_2 value of 0.09 corresponds to the uncoated version of the device (under the assumption of 30% reflection at each facet), and was also included in the experiments.

Figs. 4*a* and *b* show the relation between facet coatings, wavelength and temperature for the FP lasers with constant cavity length. A parabolic dependence was observed in the relation

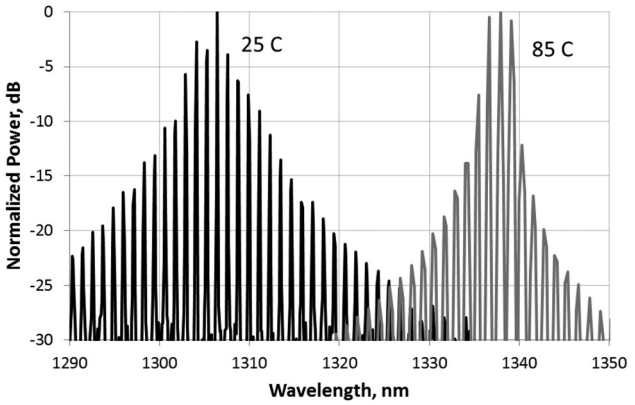

Fig. 3 *FP laser spectra measured at heat sink temperature of 25°C and 85°C*

© The Institution of Engineering and Technology 2015

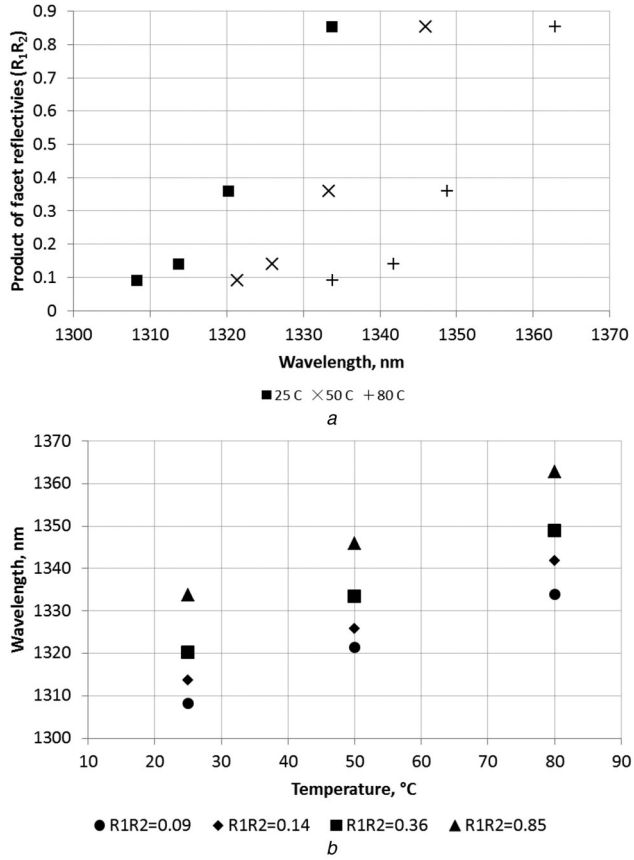

Fig. 4 *Measurements of several FP lasers with 200 μm cavity lengths*
a Wavelength against facet reflectivity
b Temperature against wavelength

between wavelength and reflectivity (Fig. 4*a*), while a more linear dependence was observed between temperature and wavelength (Fig. 4*b*).

The wavelength tuning effect observed in Fig. 4*a* is related to the reduction of losses within the laser cavity that follows the increase of the reflectivity product because of the facet coatings. This reduction of losses produces a shift of the laser Fermi level to lower energies [11], which consequently reduce the energy of the photon emission and increases its wavelength. By tailoring the facet coating reflectivity of a laser, Sacher *et al.* [11] demonstrated that it is not only possible to shift a laser wavelength, but also to change the energy level from which the photon emission takes place.

The linear dependence observed between the laser temperature and wavelength operation observed in Fig. 4*b* can be explained as a consequence of the linear variation of the laser effective mode index with temperature [12]. The rate of wavelength shift against temperature $d\lambda/dT$ for each facet coatings (0.47 nm/°C for $R_1R_2 = 0.09$, 0.51 nm/°C for $R_1R_2 = 0.14$, 0.52 nm/°C for $R_1R_2 = 0.36$ and 0.53 nm/°C for $R_1R_2 = 0.85$) is commensurate with values reported in the literature (e.g. 0.5 nm/°C, in [12]).

Given that HR coatings have a tendency to increase the wavelength output at high temperatures, it is necessary to find a compromise to constrain the laser wavelength below 1350 nm. This limit is a common industrial requirement for uncooled communication applications at 10 Gbps.

4 Ridge waveguide FP laser dynamics

The modulation bandwidth of an FP laser is mainly determined by the device resonance or relaxation frequency (f_r) at a given injection current [10]. RF parasitic elements such as the series resistance and capacitance (RC time constant) also affect the

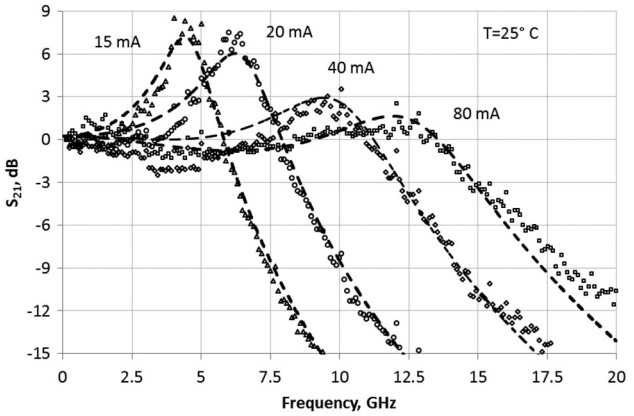

Fig. 5 *Measured electro-optical response S_{21} (markers) and model (dashed lines) of a directly modulated 200 μm cavity length FP laser*

roll-off of the electro-optical response (S_{21}), but play a less substantial role in determining the device modulation bandwidth when the waveguide cavity is short (<250 μm) and the data rate frequencies are near or below 10 Gbps.

The resonance frequency is determined by several physical parameters of the FP laser: the recombination and photon life time constants, the threshold constant of the active region, the optical gain, the steady-state photon density and the temperature [10]. To separate the intrinsic laser electro-optical response from the effect of test sub-mount and RF parasitics that do not change as a function of threshold current, a method of subtraction is usually applied [13]. The resonance frequencies of the laser can then be obtained through curve fitting techniques of the intrinsic electro-optical response.

Fig. 5 shows the measured S_{21} for a 200 μm cavity length FP laser with the product of facet coatings $R_1R_2 = 0.14$. The laser was attached to a high speed AlN sub-mount with eutectic bonding, wire bonded and tested using a high speed micro-probe input and a lensed fibre output. The electro-optical response was measured using an Agilent Network Analyzer E8361a, and the high speed 1.3 μm photo-detector u^{2}t xpdv2320r.

4.1 FP laser small signal equivalent circuit model

The electro-optical response of a laser can be described in terms of an equivalent circuit model based on lumped electrical elements. The works in [14, 15] demonstrated how the dynamics of a semi-conductor laser can be modelled by means of a network of resistances, capacitances and inductances. Given that the elements affecting the high speed electro-optical response of a laser are not exclusive to the process technique used (ridge waveguide, buried hetero-structure) or the presence of a grating (DFB), the model in [14, 15] is implemented here for the case of the 10 Gbps FP device.

Fig. 6 shows a schematic diagram of the FP laser dynamics equivalent circuit model. Circuit elements R_s and C_s are relevant to describe the laser response roll-off at high frequencies [14]. Resistances R_1, R_{s1} and R_{s2} affect the damping of the transmitted

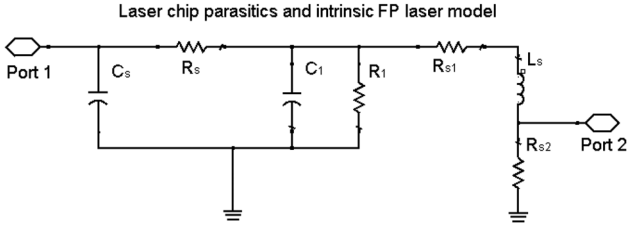

Fig. 6 *Equivalent circuit model of a high speed FP laser used to calculate the electro-optical transmission response*

© The Institution of Engineering and Technology 2015

Table 1 Laser chip parasitics and intrinsic FP laser model elements

Injection current, mA	C_s, pF	R_s, Ω	C_1, pF	R_1, Ω	R_{s1}, mΩ	R_{s2}, μΩ	L_s, pH
15	3	10.5	620	0.72	16.5	17.9	1.95
20	3	10.5	420	0.72	16.5	17.9	1.43
40	3	10.5	320	0.72	16.5	17.9	0.78
80	3	10.5	240	0.72	16.5	17.9	0.65

signal observed at the resonance frequency. Capacitance C_1 and inductance L_s determine the value of the resonance frequency, and are given by [14]

$$C_1 \simeq \tau_n q I_{tA}/2kT \tag{1}$$

$$L_s \simeq 2kT\tau_p/qI_{tA}g_0\tau_n S_0 \tag{2}$$

$$f_r \simeq 1/\left[2\pi(L_s C_1)^{0.5}\right] \tag{3}$$

where τ_n and τ_p are the laser recombination and photon life time constants, respectively, I_{tA} is the threshold constant of the active region, g_0 is an optical gain constant, S_0 is the steady-state photon density, k is the Boltzmann constant, q is the electron charge and T is the temperature.

Table 1 shows the circuit component values used to model the measured FP laser responses S_{21} that are shown in Fig. 5 for the case of four different injection currents. It can be seen in Fig. 5 that higher injection currents produce a peak S_{21} response at higher frequency values, which correspond roughly to the laser resonance frequency f_r for each case [10]. The device represented in the model and experiments corresponds to a 200 μm cavity length laser, with a product of facet reflectivity $R_1R_2 = 0.14$ operating at room temperature ($T = 25$°C). Table 1 lists the four injection currents and the circuit components used to represent the dynamic behaviour of the device for that particular situation: neither the parasitic elements (R_s, C_s) nor the resistive components of the intrinsic laser model (R_1, R_{s1}, R_{s2}) change with increased injection current. Only the elements that directly correlate with a change in the resonance frequency of the laser f_r (C_1 and L_s in (3)) change with the increasing values of injected current. The RF tool of the computer software Matlab® was used to generate and plot the modelled S_{21} responses.

The known physical design parameters of the laser, together with the obtained fitting parameters of C_1 and L_s can be used to estimate the carrier lifetime τ_n and the optical gain constant from (1) and (2). The current threshold I_{tA} is known from measurements on the laser power against current plots ($I_{tA} = 10$ mA, Fig. 2). The photon lifetime τ_p can be obtained from the parametric relations reported in [16] using the laser internal loss ($\alpha_i = 8$ cm^{-1}) known from the static operation laser model; the group velocity ($v_g = 9.1 \times 10^9$ cm/s) taken from the AlGaInAs device in [16]; and the laser facet reflectivity product $R_1R_2 = 0.14$. The photon density S_0 can be also obtained from the parametric relations in [16] using the laser confinement factor ($\Gamma = 11\%$) known from the laser device optical propagation model; the power output at a given current (Fig. 2); the active region volume; the group velocity v_g in [16]; the mirror loss ($\alpha_m = 49$ cm^{-1}) calculated from the facet reflectivity and the cavity length; and the laser output wavelength ($\lambda = 1310$ nm). For an injection current of 40 mA, for example, the calculated values of the photon lifetime and photon density were $\tau_p = 1.92$ ps and $S_0 = 4.73 \times 10^{14}$ cm^{-3}, respectively.

Using all the physical parameters mentioned in the previous paragraph as well as the fitting parameters C_1 and L_S, the calculated optical gain in (2) (at an injection current of 40 mA) is $g = g_0/v_g = 18 \times 10^{-16}$ cm^2, which is commensurate to values previously reported in the literature ($g = 9.2 \times 10^{-16}$ cm^2 in [16], for a longer AlGaInAs 400 μm cavity laser).

The carrier lifetime in this work calculated from the S_{21} response fitted value of C_1 and (1) (at an injection current of 40 mA) is $\tau_n = 1.8$ ns. This physical parameter is usually reported in the literature after measurements that take place below the laser threshold current. The value of τ_n in this work is within the order of magnitude reported in [17] at very low injection currents. Lower carrier lifetime values have been reported in the literature at threshold ($\tau_n < 0.2$ ns in [16, 17]), however for high speed laser operation above threshold, a high carrier lifetime does not have a direct impact over the resonance frequency f_r calculated from (3), given that multiplication of the expressions for L_s and C_1, eliminates the dependence of f_r on $\tau_n\left(f_r \simeq (1/2\pi)(g_0 S_0/\tau_p)^{0.5}\right)$.

Given that the laser maximum modulation bandwidth (BW_{max}) is known to increase proportionally with resonance frequency $BW_{max} \simeq 1.41 f_r$ [10], it is then important to minimise C_1 and L_s in (3) by means of the physical parameters determining their values in (1) and (2). Thus, varying cavity length, facet coatings and temperature has a direct impact on C_1 and L_s. In the following sections the effects of those changes in the resonance frequency are evaluated to optimise and validate a high speed FP laser design. This will guarantee that the modulation bandwidth will be sufficiently high (>10 GHz) when the injection current is near 40 mA, a requirement for power specification limitations in communication applications.

4.2 Subtraction method

The f_r parameter extraction method implemented in this work [13] consists of measuring S_{21} at several injection currents, subtracting the response of the lowest injection current from the responses with the higher injection currents, and finally curve fitting these plots to a parametric equation. The fitting equation is given by [13] (see (4))

$$\text{Response}(f) = 10\log_{10}\left(\frac{f_{r1}^4}{(f^2 - f_{r1}^2)^2 + (\Gamma_{d1}/2\pi)^2 f^2} \cdot \frac{(f^2 - f_{r0}^2)^2 + (\Gamma_{d0}/2\pi)^2 f^2}{f_{r0}^4}\right) \tag{4}$$

where f_{r1} and f_{r0} are the resonance frequencies at the higher and lower injection current to be extracted, Γ_{d1} and Γ_{d0} are the corresponding damping factors, and f is the modulation frequency. The curve fitting tool of the commercial software Matlab® was used to extract the relevant parameters for each device. A database was formed with all the parameters extracted from the S_{21} measurements. Responses were measured for FP laser devices with different cavity lengths, facet coating reflectivities and subject to different heat sink temperatures. Resonance frequencies and damping factors were extracted from each measurement. This study, however, is focused on the laser design variation effect on the value of the slope of resonance frequency against square root of the injection current, also called the modulation efficiency.

4.3 Resonance frequency and facet coating

Cheng *et al*. [18] have argued that the optimal laser facet coating that achieves the highest modulation efficiency has a reflectivity product value close to that of the uncoated facets (Demonstrated for the InGaAsP system in [18]). In [18] they presented calculation of the squared resonance frequency f_r^2 as a function of the facet reflectivity using a set of equations that include the effect of the lowering of the S_{21} peak frequency because of damping, by substitution of an expression of linear differential gain g by the non-linear expression $g/(1 + \varepsilon S)$. Their plot in [18] showed that for the case of typical non-linear gain suppression values ($\varepsilon = 2.4 \times 10^{-23}$ m^3) the maximum resonance frequency would be obtained for facet reflectivity values close to the uncoated as-cleaved values ($R_1R_2 = 0.09$). Higher reflectivity facet coating results in higher modulation bandwidths only when the bias current is comparable

© The Institution of Engineering and Technology 2015

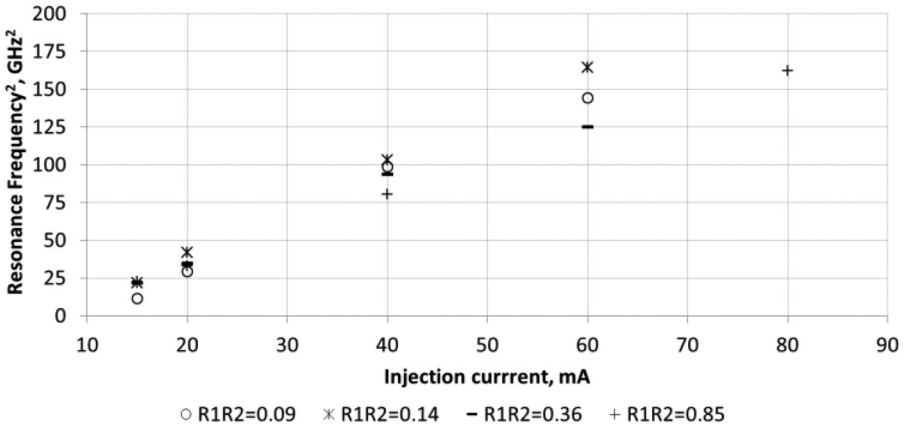

Fig. 7 *Measurement of square resonance frequency against injection current of FP lasers with four different values of facet reflectivity (T = 25°C)*

with threshold. Gain saturation and damping of the laser response lowered the values of resonance frequency under high bias current operation.

In contrast to the results in [18], Mar *et al*. [19] have argued that the main limiting factor of the modulation bandwidth is the heating because of the injection current required to operate the laser. Their experimental results in [19] showed that, even for high bias current, it is possible to obtain high resonance frequencies by increasing one of the facets reflectivity value (from the single uncoated facet value of 30% to the high reflectivity value of 90%). For uncooled applications, it is important to reduce the value of the threshold across temperature while increasing the characteristic temperature (T_0) of the lasers, and for that reason it has become the norm the use of front and back coatings with high reflectivity values [19].

In this work, confirmation of the results in [18] is shown for the case of the strained AlGaInAs epitaxial laser system. At higher bias currents, higher resonance frequencies are observed for the coating values nearer to the as-cleaved values ($R_1R_2 = 0.09$, $R_1R_2 = 0.14$). High facet reflectivity values ($R_1R_2 = 0.36$, $R_1R_2 = 0.85$) show only a marginal resonance frequency improvement over the as-cleaved samples when the bias current is close to the threshold values.

The square of the resonance frequency against absolute injection current is shown in Fig. 7 for FP devices with 200 µm long cavities and four different sets of facet coatings. These experiments confirm the argument in [18] that the highest values of f_r^2 are obtained for device facet reflectivity close to the uncoated values.

The threshold currents for the devices in these experiments were 11 mA ($R_1R_2 = 0.09$), 10 mA ($R_1R_2 = 0.14$), 7.5 mA ($R_1R_2 = 0.36$) and 5.4 mA ($R_1R_2 = 0.85$).

4.4 Resonance frequency and temperature

The coatings that showed the highest resonance frequencies in the previous sections were used to design three different FP lasers with different cavity lengths. The devices were sub-mounted and placed on a brass stage that was controlled to perform dynamic measurements across several values of temperature. A high speed microprobe and a lensed fibre were used to measure the electro-optical response (S_{21}) as described earlier. Resonance frequency values were extracted from S_{21} and plotted against the square root of injected current for each temperature.

Fig. 8*a* shows the measured resonance frequency values for an uncoated FP laser with a 160 µm cavity length. The solid line in the plot corresponds to the value of the highest modulation efficiency (2.3 GHz/mA$^{0.5}$) obtained by linearly fitting the measured ratio of f_r to $(I\text{-}I_{th})^{0.5}$ at the lowest temperature of 15°C. The dashed line corresponds to the value of the lowest modulation efficiency (1.56 GHz/mA$^{0.5}$) obtained with a similar linear fit at the highest temperature of 75°C.

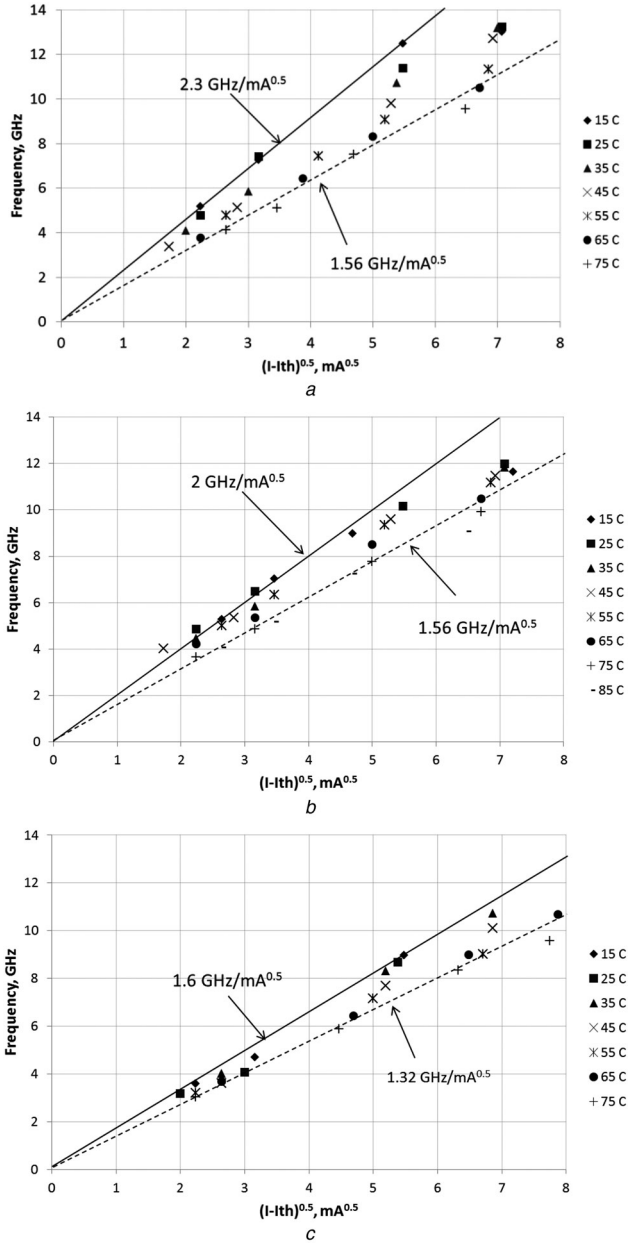

Fig. 8 *Measured resonance frequency against injection current for FP lasers with cavity lengths of*

a 160 µm
b 200 µm
c 250 µm

© The Institution of Engineering and Technology 2015

Dynamic measurements of FP lasers with cavity lengths of 200 and 250 μm are shown in Figs. 8*b* and *c*. The coatings used for these two devices was $R_1R_2 = 0.14$, which is slightly higher than the uncoated version used with the 160 μm device. The linear plots were obtained with the same procedure described above.

The experimental results clearly show that the FP lasers with the shorter cavity length are more efficient at modulating high speed signals across temperature. However, the change in modulation efficiency is larger (0.74 GHz/mA$^{0.5}$) for the case of the 160 μm cavity length compared with the 250 μm cavity length (0.28 GHz/mA$^{0.5}$), when the temperature varies from 15°C to 75°C.

To demonstrate the application of these FP laser designs for data transmission, a bit error rate test kit was used to drive the laser while the eye diagram of the modulated light signal was captured using a fast oscilloscope. The measurements were performed for an FP laser device with a cavity length of 200 μm and facet coating values of $R_1R_2 = 0.14$.

Screen shots of the fast oscilloscope used to test the laser are shown in Figs. 9*a* and *b*, which corresponds to test temperatures of 25°C and 85°C. In both cases the eyes appear wide open with a 10 Giga-bit Ethernet (10GBE) mask margin of 27 and 37%, respectively.

These measurements took place using a DC injection current of 40 mA. The eye rise time and fall time were approximately 40 ps and 50 ps, respectively, for each temperature. The quality of the eye was optimised by adjusting the modulating high speed driver current swing until a 4 dB extinction ratio was achieved.

Initial reliability tests for the FP laser device with 200 μm cavity length and coatings with $R_1R_2 = 0.14$ have been performed. The accelerated life test consists of a sample of 20 devices subjected to a temperature of 70°C and constant injection current of 50 mA. Using a failure condition of 50% change in the laser operation current required at each test point in time (10 mW of intensity output power), no device failures have been yet observed after 1500 h of accelerated test.

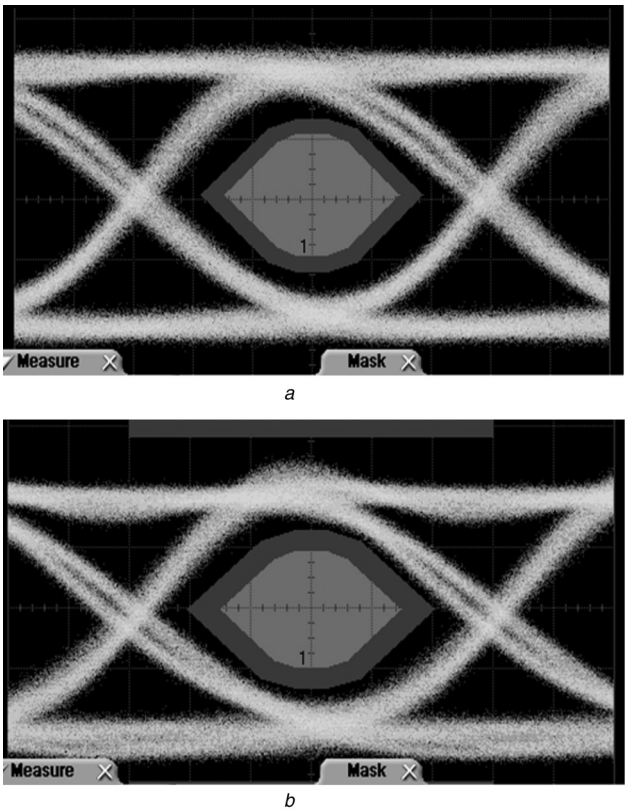

Fig. 9 *Screen shot of modulated high speed FP laser eye diagram measured at the temperature of*

a 25°C
b 85°C

5 Conclusions

In this study we have experimentally shown how parameters such as cavity length, facet coating and temperature affect the modulation efficiency performance of high speed FP lasers based on the strained AlGaInAs-InP epitaxial system. Shorter cavity lengths (<200 μm) were demonstrated to be the best option for high speed operation, as long as the active layer region contains enough number of stacked quantum wells. Facet coat reflectivity close to the uncoated facet values ($R_1R_2 = 0.14$) showed to produce the highest values of resonance frequency at room temperature, but at the cost of increased threshold currents when high temperature operation is required (Ith = 19 mA at 85°C). Increasing the reflectivity of the coatings from $R_1R_2 = 0.09$ to $R_1R_2 = 0.85$ also showed an increase of the laser wavelength by more than 25 nm, independently of the temperature of operation. These effects have to be carefully accounted for to secure uncooled operation of the lasers in the allocated channels for communication applications.

Eye diagrams for an FP device 200 μm long with $R_1R_2 = 0.14$ coatings were shown to comply with 10 GBE mask tests at temperatures of 25°C and 85°C showing margins of 27 and 37%, respectively. Initial reliability accelerated tests have been performed at a temperature of 70°C with 50 mA injection current. No failures have been observed in a sample of 20 FP devices after 1500 h of accumulated test.

6 Acknowledgments

This work was supported by the Knowledge Transfer Partnership 8847-Development of a high performance, low cost, single frequency laser device platform for next generation access networks.

7 References

1 Nakahara, K., Tsuchiya, T., Nomoto, E., Mukaikubo, M.: 'Transmission properties of 1.3-μm InGaAlAs MQW FP lasers in 10-Gb/s uncooled operation', *IEEE J. Lightwave Technol.*, 2005, **23**, (12), pp. 3997–4003
2 Paoletti, R., Agresti, M., Bertone, D., *et al.*: 'Highly reliable and high-yield 1300-nm InGaAlAs directly modulated ridge Fabry–Pérot lasers, operating at 10-Gb/s, up to 110°C, with constant current swing', *J. Lightw. Technol.*, 2006, **24**, (1), pp. 143–149
3 Nakahara, K., Tsuchiya, T., Kitatani, T., *et al.*: '12.5-Gb/s direct modulation up to 115°C in 1.3-μm InGaAlAs-MQW RWG DFB lasers with notch-free grating structure', *IEEE J. Lightwave Technol.*, 2004, **22**, (1), pp. 159–165
4 Klotzkin, D., Kojima, K., Jordache, N., *et al.*: 'High-speed directly modulated Fabry–Pérot and distributed-feedback spot-size-converted lasers suitable for passive alignment, unisolated operation, and uncooled environments up to 85° C', *IEEE J. Lightwave Technol.*, 2003, **21**, (1), pp. 69–78
5 Williams, K.A., Penty, R.V., White, I.H., Silver, M.: 'Requirements for uncooled direct laser modulation at 10 Gb/s'. Proc. SPIE 4287, In-Plane Semiconductor Lasers V, 2001, pp. 118–127
6 Selmic, S.R., Chou, T.-M., Sih, J.P., *et al.*: 'Design and characterization of 1.3-μm AlGaInAs-InP multiple-quantum-well laser', *IEEE J. Sel. Topic Quantum Electron.*, 2001, **7**, (2), pp. 340–348
7 Yamamoto, T.: 'High-speed directly modulated lasers'. Proc. Opt. Fiber Commun. Conf., Los Angeles, CA, USA, 2012, OTH3F5
8 Coldren, L.A., Corzine, S.W.: 'Dynamic effects', in Chang, K. (Ed.): 'Diode lasers and photonic integrated circuits' (Wiley, USA, 1995, 1st edn.), pp. 241–245
9 Agrawal, G.P., Dutta, N.K.: 'Recombination mechanisms in semiconductors', in Mitra, S. (Ed.): 'Long-wavelength semiconductor lasers' (Van Nostrand Reinhold, USA, 1986, 1st edn.), pp. 84–94
10 Tucker, R.S.: 'High-speed modulation of semiconductor lasers', *IEEE J. Lightwave Technol.*, 1985, **LT-3**, pp. 1180–1192
11 Sacher, J., Elsasser, W., Gobel, E.O., Jung, H.: 'Tailoring of quantum well laser emission wavelength by antireflection facet coating', *Electron. Lett.*, 1991, **27**, (16), pp. 1463–1464
12 Agrawal, G.P., Dutta, N.K.: 'Distributed-feedback semiconductor lasers', in Mitra, S. (Ed.): 'Long-wavelength semiconductor lasers' (Van Nostrand Reinhold, USA, 1986, 1st edn.), pp. 314–318
13 Morton, P.A., Tanbun-Ek, T., Logan, R.A., Sergent, A.M., Sciortino, P.F. Jr., Coblentz, D.I.: 'Frequency response subtraction for simple measurement of intrinsic laser dynamic properties', *IEEE Photon. Technol. Lett.*, 1992, **4**, (2), pp. 133–136
14 Tucker, R.S., Kaminow, I.P.: 'High-frequency characteristics of directly modulated InGaAsP ridge waveguide and buried heterostructure lasers', *J. Lightwave Technol.*, 1984, **LT-2**, pp. 385–393
15 Lee, J., Nam, S., Lee, S.H., Jeong, J.: 'A complete small-signal equivalent circuit model of cooled butterfly-type 2.5 Gbps DFB laser modules and its application to

© The Institution of Engineering and Technology 2015

improve high frequency characteristics', *IEEE Trans. Adv. Packag.*, 2002, **25**, (4), pp. 543–548
16 Liu, G., Chuang, S.L.: 'High-speed modulation of long-wavelength $In_{1-x}Ga_xAs_yP_{1-y}$ and $In_{1-x-y}Ga_xAl_yAs$ strained quantum-well lasers', *IEEE J. Quantum Electron.*, 2001, **37**, (10), pp. 1283–1291
17 Houle, T.J., Yong, J.C.L., Marinelli, C.M., *et al.*: 'Characterization of the temperature sensitivity of gain and recombination mechanisms in 1.3-μm AlGaInAs MQW lasers', *IEEE J. Quantum Electron.*, 2005, **41**, (2), pp. 132–139
18 Cheng, W.-H., Mar, A., Bowers, J.E., Huang, R.T., Su, C.B.: 'High-speed 1.3 μm InGaAsP Fabry-Péatrot lasers for digital and analog applications', *IEEE J. Quantum Electron.*, 1993, **29**, (6), pp. 1660–1667
19 Mar, A., Morton, P.A., Bowers, J.E.: 'Optimum facet reflectivity for high speed lasers', *Electron. Lett.*, 1990, **26**, (17), pp. 1382–1384

© The Institution of Engineering and Technology 2015